IET Radar, Sonar & Navigation

Research Article

IET Journals
The Institution of Engineering and Technology

SFMM design in colocated CS-MIMO radar for jamming and interference joint suppression

ISSN 1751-8784
Received on 11th October 2017
Revised 13th March 2018
Accepted on 15th March 2018
E-First on 17th April 2018
doi: 10.1049/iet-rsn.2017.0444
www.ietdl.org

Wei Xiong[1,2], Maria Greco[3], Fulvio Gini[3], Gong Zhang[1] ✉, Zhenni Peng[4]

[1] *Key Laboratory of Radar Imaging and Microwave Photonics, Ministry of Education, Nanjing University of Aeronautics and Astronautics, Nanjing 211106, People's Republic of China*

[2] *Leihua Electronic Technology Research Institute, Aviation Industry Corporation of China, Wuxi 214063, People's Republic of China*

[3] *Dipartimento di Ingegneria dell' Informazione, University of Pisa, Pisa 56122, Italy*

[4] *Key Laboratory of Advanced Technology for Small and Medium-sized UAV, Ministry of Industry and Information Technology, Nanjing 210016, People's Republic of China*

✉ *E-mail: gzhang@nuaa.edu.cn*

Abstract: This study focuses on the problem of joint suppression of active jamming in target sector-of-interest (SOI) and out-of-sector interference for colocated compressive sensing multiple-input–multiple-output (CS-MIMO) radar. Three effective strategies for spatial filter measurement matrix (SFMM) design are outlined. Unlike the previous reported Capon beamformer and minimum variance distortionless response beamformer, the proposed design strategies only depend on the target spatial SOI rather than the accurate directions-of-arrival (DOAs) of targets, jammers and interfering sources to obtain deep nulls or notches for the SOI jamming and low-attenuation levels for the out-of-sector interference. The SFMM design criteria are derived using the second-order cone programming and solved as convex optimisation problems. The proposed approaches can simultaneously suppress the SOI jamming and attenuate the out-of-sector interference. Meanwhile, better DOA estimation accuracy can be achieved. Simulation results demonstrate the superiority of the proposed approaches over the other methods for colocated CS-MIMO radar.

1 Introduction

Unlike the distributed multiple-input–multiple-output (MIMO) radar, the antennas in colocated MIMO radar are closely spaced so that, in the far-field, they look at the target under the same aspect and, contrary to the phased array (PA) systems, waveform diversity allowed by the transmit and receive arrays can be exploited [1, 2]. It has been shown that the colocated MIMO radars have some advantages over PA radars such as the extended virtual array aperture, the increased upper limit on the number of detectable targets, improved parameter identifiability and angular resolution and so on [1–5]. In the last decade, by exploiting the target sparsity in the target space/scene, compressive sensing (CS) theory has been successfully applied to MIMO radars and has shown great potentials in target parameter estimation [6], Synthetic Aperture Radar (SAR) imaging [7], waveform design [8] and interference attenuation [9]. CS-MIMO radar systems have been proposed in [6–8] and the beamforming techniques for colocated CS-MIMO radars have also been studied to achieve processing gain or the desired beampattern to suppress the target-like interference [9, 10]. Colocated CS-MIMO radar can achieve either the same localisation performance as traditional methods with significantly fewer measurements or significantly improved performance with the same number of measurements [10]. However, the assumed target sparsity decreases in the presence of clutter, interference and jamming, and the parameter estimation performance would degrade severely. Yu *et al.* [10] proposed a Capon-like beamforming method to suppress clutter in the context of colocated CS-MIMO radar. However, when the clutter covariance and directions-of-arrival (DOAs) of interfering sources and/or jammers are unknown, conventional methods such as the Capon beamformer [10] and the minimum variance distortionless response beamformer of [11, 12] fail. Without prior knowledge of the clutter covariance function, the Capon beamforming does not enable to improve the DOA estimation performance of colocated CS-MIMO radar. Under the assumption of known spatial sector-of-interest (SOI), where the targets are likely to be located, Hassanien and Vorobyov [4] proposed a transmit beamspace energy focusing technique for colocated MIMO radars with application to DOA finding for multiple targets and simultaneously suppressing the interference and clutter out of the spatial SOI. Spheroidal sequences were employed to design the transmit beamspace matrix so that the ratio of the energy radiated within the desired spatial SOI to the total radiated energy was maximised [4]. For a better DOA estimation of colocated MIMO radar in the presence of interference and jamming, Li *et al.* [13] proposed three reduced dimension beamspace matrices to achieve reasonable tradeoffs between the desired SOI source distortion and the out-of-sector interference/jamming (possibly in-sector) attenuation. However, the beamspace matrix was developed by minimising the output power of the total received signal followed by a transformation. The transformed target signal would be also attenuated while minimising the power of the transformed interference and jamming. Similarly, Tao *et al.* [9] proposed a spatial filter measurement matrix (SFMM) design method for colocated CS-MIMO radar based on the pass-band beamforming for spatial target sectors and lower gain beamforming for out-of-sector areas to suppress the possible interference or clutter. However, it can be seen that the attenuation levels for spatial areas out-of-sector are limited. Only if the interference-to-noise ratio (INR) or clutter-to-NR (CNR) is small, the out-of-sector interference or clutter would be suppressed. Moreover, the case of possible jamming in the SOI is not considered. Actually, with the development of electronic countermeasure (ECM), the important target is often protected by the countermeasure system to prevent radars from operating as well as possible.

As an important ECM, active jamming often takes the form of high-power transmission and blocks the radar receive system with highly concentrated energy [14]. In view of the closed element spacing of transmit and receive arrays, colocated CS-MIMO radars can be blocked by active jamming. Moreover, terrain-scattered jamming also is a typical active jamming example, which occurs in a dispersive manner when the ground reflects the power transmitted by a high-power jammer [11, 15]. It shows up as a

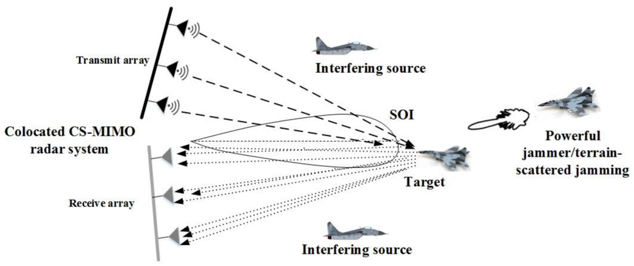

Fig. 1 *Traditional scenario of SOI jammer and out-of-sector interfering sources*

distributed source in the target SOI, even in the same direction as the desired target, and it severely affects target's DOA estimation performance of conventional methods. To the best of our knowledge, so far an efficient approach of active jamming and interference joint suppression has not been investigated for the target's DOA estimation in colocated CS-MIMO radar.

Different from the target-like interference, the active jamming always comes from the directly radiated or the ground-reflected signal of jammers, but does not originate from the MIMO radar transmit array, so the informations on transmit antennas are not included in the received jamming. As shown in Fig. 1, we address the problem of the joint suppression of powerful active jamming in target SOI and out-of-sector interference/clutter for colocated CS-MIMO radar. Inspired by papers [4, 13], and considering the differences between interference and active jamming described above, we adopt the first two beamspace matrix optimisation schemes for colocated MIMO radar of [13] and propose here three adaptive SFMM design strategies for the general case of unknown SOI jamming and/or out-of-sector interference/clutter in the context of colocated CS-MIMO radar. As for the spheroidal sequences based beamspace matrix (SSBM) of [4], the SFMM design criterion is derived using the second-order cone (SOC) programming and solving a convex optimisation problem.

The remainder of this paper is organised as follows. Section 2 presents the signal model of colocated CS-MIMO radar in the presence of active jamming and interference. In Section 3, first a brief introduction to the SSBM design method is provided, then three adaptive SFMM design approaches are proposed. Numerical analysis and comparison results are given in Section 4. Finally, we make some concluding remarks in Section 5.

Notations: The bold upper and lower case symbols are employed to denote the matrices and vectors, respectively. The transpose and Hermitian transpose operations are represented as $(\cdot)^{\mathrm{T}}$ and $(\cdot)^{\mathrm{H}}$. $\otimes$ symbolises Kronecker product. $\|\cdot\|_2$ and $\|\cdot\|_{\mathrm{F}}$ present Euclidean norm and Frobenius norm. $\mathrm{vec}(\boldsymbol{A})$ stands for the operator that stacks the columns of a matrix $\boldsymbol{A}$ into one column vector. $\boldsymbol{I}$ refers to the identity matrix. $\mathbf{1}_M$ is the $M \times 1$ vector of all ones. $\cup$ is the union operation of sets and the statistical expectation is represented by $E\{\cdot\}$.

2 Signal model for colocated CS-MIMO radar

2.1 Conventional signal model

Consider a colocated CS-MIMO radar system equipped with a transmit uniform linear array (ULA) of M ($M \geq 2$) antenna elements and a receive ULA of N ($N \geq 2$) antenna elements. Transmit and receive arrays are assumed to be closely located so that a target located in the far-field shares an identical spatial angle. It is assumed that K sources are measured in a noise background. With the azimuth angle ϕ_k ($k = 1, 2, \ldots, K$) of the kth source, the transmit steering vector and receive steering vector are denoted as

$$\boldsymbol{a}(\phi_k) = \left[1, \mathrm{e}^{\mathrm{j}2\pi d/\lambda \sin\phi_k}, \ldots, \mathrm{e}^{\mathrm{j}2\pi(M-1)d/\lambda \sin\phi_k}\right]^{\mathrm{T}} \in \mathbb{C}^{M \times 1} \tag{1}$$

$$\boldsymbol{b}(\phi_k) = \left[1, \mathrm{e}^{\mathrm{j}2\pi d/\lambda \sin\phi_k}, \ldots, \mathrm{e}^{\mathrm{j}2\pi(N-1)d/\lambda \sin\phi_k}\right]^{\mathrm{T}} \in \mathbb{C}^{N \times 1} \tag{2}$$

where $a_m(\phi_k) = \mathrm{e}^{\mathrm{j}2\pi(m-1)d/\lambda \sin\phi_k}$, $b_n(\phi_k) = \mathrm{e}^{\mathrm{j}2\pi(n-1)d/\lambda \sin\phi_k}$ are the elements of $\boldsymbol{a}(\phi_k)$ and $\boldsymbol{b}(\phi_k)$, respectively. λ is the radar wavelength. d refers to the distance between two adjacent elements and $d \leq \lambda/2$ for non-ambiguous [16]. Herein, it is always set as $d = \lambda/2$ for derivation simplicity [4, 11]. The M transmit antennas are used to transmit orthogonal waveforms. Let $\boldsymbol{s}_m(t)$ ($m = 1, 2, \ldots, M$) denote the baseband signal transmitted by the mth transmitter, which is assumed to be orthogonal to the others with power equal to 1, *i.e.* $\int_{T_{\mathrm{p}}} \boldsymbol{s}_{\mathrm{p}}(t)\boldsymbol{s}_q^*(t)\,\mathrm{d}t = \delta[p-q]$, $p, q = 1, 2, \ldots, M$, where T_{p} is the pulse duration and $\delta[\cdot]$ is Kronecker's delta function. The matrix of transmitted signals is given by $\boldsymbol{S}(t) = [\boldsymbol{s}_1(t), \boldsymbol{s}_2(t), \ldots, \boldsymbol{s}_M(t)]$. Under the same assumption as in [14], the target, interfering sources and jammers are static, so the Doppler frequency is not considered in our signal model. Then, the received echo $\boldsymbol{x}_n(t, \tau)$ of the nth receiver at the fast time t within the τth pulse can be expressed as [9]

$$\boldsymbol{x}_n(t, \tau) = \sum_{k=1}^{K} \alpha_k(\tau) b_n(\phi_k) \boldsymbol{S}(t) \boldsymbol{a}(\phi_k) + \boldsymbol{n}(t) \tag{3}$$

where $\tau = 1, 2, \ldots, L_{\mathrm{s}}$ is the slow-time (pulse) index, $\alpha_k(\tau)$ is the complex amplitude of the kth source with variance σ_k^2. It is emphasised that $\alpha_k(\tau)$ is assumed to be constant during the whole pulse, but varies independently from pulse to pulse, *i.e.* it obeys the Swerling II model. $\boldsymbol{n}(t)$ denotes the zero-mean Gaussian noise process with variance σ_{n0}^2. Suppose that the K sources include K_{T} targets and K_{I} interfering sources, *i.e.* $K = K_{\mathrm{T}} + K_{\mathrm{I}}$. Moreover, there are J active jammers or terrain-scattered jamming located at directions ϕ_j, $j = 1, 2, \ldots, J$, and the jamming signal is $\boldsymbol{J}_j(t)$. Then, (3) can be rewritten as (4). Defining the fast-time snapshot (sample) number of a pulse as L_{f}, then the sampled received echo is given by (5), where $\alpha_r(\tau)(r = 1, 2, \ldots, K_{\mathrm{T}})$, $\alpha_i(\tau)$ ($i = 1, 2, \ldots, K_{\mathrm{I}}$) denote the complex amplitudes, ϕ_r and ϕ_{i} are the DOAs of the rth target and the ith interfering source, $\beta_j(\tau)$ is the complex amplitude of the jth jammer, $\boldsymbol{n}$ denotes the $L_{\mathrm{f}} \times 1$ noise and $\boldsymbol{S}$ and $\boldsymbol{J}_j$ are the $L_{\mathrm{f}} \times M$ sampled MIMO radar signal matrix and the jth jammer matrix, respectively. Herein, $\mathbf{1}_M$ is the jammer transmit steering vector, because the jammer is independent of the radar transmit array [11, 13, 14]

$$\begin{aligned}\boldsymbol{x}_n(\tau, t) = &\sum_{r=1}^{K_{\mathrm{T}}} \alpha_r(\tau) b_n(\phi_r) \boldsymbol{S}(t) \boldsymbol{a}(\phi_r) \\ &+ \sum_{i=1}^{K_{\mathrm{I}}} \alpha_i(\tau) b_n(\phi_i) \boldsymbol{S}(t) \boldsymbol{a}(\phi_i) \\ &+ \sum_{j=1}^{J} \beta_j(\tau) b_n(\phi_j) \boldsymbol{J}_j(t) \mathbf{1}_M + \boldsymbol{n}(t)\end{aligned} \tag{4}$$

$$\begin{aligned}\boldsymbol{x}_n(\tau) = &\sum_{r=1}^{K_{\mathrm{T}}} \alpha_r(\tau) b_n(\phi_r) \boldsymbol{S} \boldsymbol{a}(\phi_r) \\ &+ \sum_{i=1}^{K_{\mathrm{I}}} \alpha_i(\tau) b_n(\phi_i) \boldsymbol{S} \boldsymbol{a}(\phi_i) \\ &+ \sum_{j=1}^{J} \beta_j(\tau) b_n(\phi_j) \boldsymbol{J}_j \mathbf{1}_M + \boldsymbol{n}\end{aligned} \tag{5}$$

$$\begin{aligned}\boldsymbol{r}_n(\tau) &= \sum_{r=1}^{K_{\mathrm{T}}} \alpha_r(\tau) b_n(\phi_r) \boldsymbol{S} \boldsymbol{a}(\phi_r) + \boldsymbol{n} \\ &= \sum_{q=1}^{Q} \gamma_q(\tau) b_n(\theta_q) \boldsymbol{S} \boldsymbol{a}(\theta_q) + \boldsymbol{n}\end{aligned} \tag{6}$$

As shown in Fig. 2*a*, the conventional DOA estimation method of colocated CS-MIMO radar has no ability to reject the DOAs of

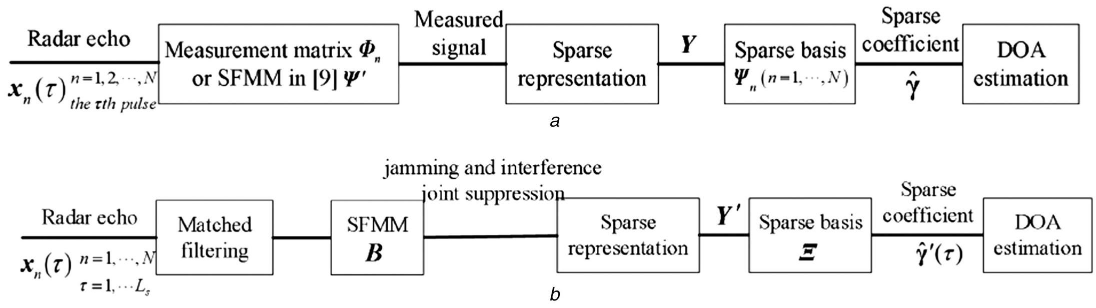

Fig. 2 *Target's DOA estimation architectures of colocated CS-MIMO radar*
(a) Conventional CS method/SFMM-based method in [9], ***(b)*** Proposed SFMM-based method for jamming and interference joint suppression

unwanted interference and jammers. The whole angle space is first discretised in a dense grid $\boldsymbol{\Omega} = [\theta_1, \theta_2, \ldots, \theta_Q]$ $(Q \gg K + J)$ so that the detectable sources are all on the grid (off-grid sources are not considered here). Then, the $L_f \times 1$ received echo vector without interference and jammers in (5) can be rewritten as (6), where

$$\gamma_q(\tau) = \begin{cases} \alpha_r(\tau) & \text{if } \theta_q = \phi_r \\ 0 & \text{otherwise} \end{cases} \tag{7}$$

For the nth receive antenna, a sparse basis $\boldsymbol{\Psi}_n$ of size $L_f \times Q$ is constructed as follows:

$$\boldsymbol{\Psi}_n = \left[b_n(\theta_1)\boldsymbol{Sa}(\theta_1),\ b_n(\theta_2)\boldsymbol{Sa}(\theta_2),\ \ldots,\ b_N(\theta_Q)\boldsymbol{Sa}(\theta_Q)\right] \tag{8}$$

The sparse representation (SR) of the $L_f \times 1$ first part $\boldsymbol{p}_n(\tau)$ on the right-hand side in (6) is given by

$$\boldsymbol{p}_n(\tau) = \boldsymbol{\Psi}_n\boldsymbol{\gamma}(\tau) \tag{9}$$

where $\boldsymbol{\gamma}(\tau) = [\gamma_1(\tau), \gamma_2(\tau), \ldots, \gamma_Q(\tau)]^{\mathrm{T}}$ is the $Q \times 1$ vector of SR-based coefficients.

Let a matrix $\boldsymbol{\Phi}_n \in \mathbb{C}^{M \times L_f}$ be the measurement matrix, which has a small correlation with $\boldsymbol{\Psi}_n$. The measured projection of $\boldsymbol{r}_n(\tau)$ can be depicted as

$$\begin{aligned} \boldsymbol{y}_n(\tau) &= \boldsymbol{\Phi}_n\boldsymbol{r}_n(\tau) = \boldsymbol{\Phi}_n(\boldsymbol{p}_n(\tau) + \boldsymbol{n}) \\ &= \boldsymbol{\Phi}_n\boldsymbol{\Psi}_n\boldsymbol{\gamma}(\tau) + \boldsymbol{n}' = \boldsymbol{T}_n\boldsymbol{\gamma}(\tau) + \boldsymbol{n}' \end{aligned} \tag{10}$$

where $\boldsymbol{T}_n = \boldsymbol{\Phi}_n\boldsymbol{\Psi}_n$ is the $M \times Q$ sensing matrix at the nth receive antenna and $\boldsymbol{n}' = \boldsymbol{\Phi}_n\boldsymbol{n}$ is the $M \times 1$ measured noise. Within the τth pulse, the projection output of N receive antennas, *i.e.* $\boldsymbol{Y} = [\boldsymbol{y}_1, \boldsymbol{y}_2, \ldots, \boldsymbol{y}_N]^{\mathrm{T}}$ with size $M \times N$, can be formulated as [9]

$$\boldsymbol{Y} = [\boldsymbol{T}_1, \boldsymbol{T}_2, \ldots, \boldsymbol{T}_N]^{\mathrm{T}}\boldsymbol{\gamma} + \boldsymbol{E} \tag{11}$$

where $\boldsymbol{\gamma}$ is the $Q \times 1$ coefficient vector and $\boldsymbol{E}$ denotes the $M \times N$ noise matrix. Stacking the matrix $\boldsymbol{Y}$ into a vector, we have

$$\begin{aligned} \boldsymbol{y} &= \mathrm{vec}(\boldsymbol{Y}) = \left[\boldsymbol{T}_1^{\mathrm{T}}, \boldsymbol{T}_2^{\mathrm{T}}, \ldots, \boldsymbol{T}_N^{\mathrm{T}}\right]^{\mathrm{T}}\boldsymbol{\gamma} + \mathrm{vec}(\boldsymbol{E}) \\ &= \boldsymbol{\Gamma}\boldsymbol{\gamma} + \boldsymbol{n}'' \end{aligned} \tag{12}$$

where $\boldsymbol{\Gamma} = \left[\boldsymbol{T}_1^{\mathrm{T}}, \boldsymbol{T}_2^{\mathrm{T}}, \ldots, \boldsymbol{T}_N^{\mathrm{T}}\right]^{\mathrm{T}}$ is the $MN \times Q$ sensing matrix of N receive antennas and $\boldsymbol{n}'' = \mathrm{vec}(\mathbf{E})$ is the $MN \times 1$ noise vector. Then, to perform DOA estimation we have to recover the sparse coefficient vector $\boldsymbol{\gamma}$ from the measurement vector $\boldsymbol{y}$. The sparse recovery problem can be formulated as an l_1-optimisation as in problem p_0 [9]. The corresponding angles with the K_T largest non-zero sparse coefficients of the recovered vector $\hat{\boldsymbol{\gamma}}$ for $\boldsymbol{\Gamma}$ provide the estimated DOAs of targets

$$p_0 = \begin{cases} \min\limits_{\gamma} & \| \boldsymbol{\gamma} \|_1 \\ \text{s.t.} & \boldsymbol{y} = \boldsymbol{\Gamma}\boldsymbol{\gamma} \end{cases} \tag{13}$$

However, in the presence of interference and jamming, the measured projection of $\boldsymbol{x}_n(\tau)$ without noise in (5) is given by the equation below:

$$\begin{aligned} \boldsymbol{y'}_n(\tau) &= \boldsymbol{r}_n(\tau) + \boldsymbol{\Phi}_n \sum_{i=1}^{K_I} \alpha_i(\tau) b_n(\phi_i)\boldsymbol{Sa}(\phi_i) \\ &\quad + \boldsymbol{\Phi}_n \sum_{j=1}^{J} \beta_j(\tau) b_n(\phi_j)\boldsymbol{J}_j\mathbf{1}_M \end{aligned} \tag{14}$$

From the last two terms, it is seen that: (a) similar to the SR of target echo, the measured interference/clutter term can also be sparsely represented by $\boldsymbol{T}_n$ and the estimated DOAs of powerful interfering sources/clutter would be probably regarded erroneously as the ones of targets; (b) the measured jamming term has no direct correlation with $\boldsymbol{T}_n$, but it can severely affect the target's DOA estimation based on the strong transmitted power; (c) the SFMM $\boldsymbol{\Psi}'$, designed as in [9], can suppress only the out-of-sector interference based on the pass-band beamformer focusing on the target SOI. Unfortunately, when the jamming appears in the SOI, as in the case of self-defense jamming and terrain-scattered jamming, the performance of target's DOA estimation can severely degrade, especially because of the powerful jammers present at the same directions as the targets. A new approach for the joint suppression of out-of-sector interference and active jamming in SOI is then necessary. The new approach for target's DOA estimation is shown in Fig. 2*b* and described in Section 3.

2.2 Signal model for interference and jamming joint suppression

To virtually extend the array aperture and increase the upper limit on the number of detectable targets, the received echo in (4) is first matched filtered to the M orthogonal waveforms $\int_{T_p} \boldsymbol{x}_n(\tau, t)\boldsymbol{S}^{\mathrm{H}}(t)\,\mathrm{d}t$ at the receiver, while the direct pulse repeater jamming is generally assumed for simplicity [11, 13], *i.e.* $\boldsymbol{J}_j(t) = \boldsymbol{S}(t)$, then we stack the matched filters' outputs into an $MN \times 1$ virtual vector as the equation below:

$$\begin{aligned} \boldsymbol{z}(\tau) &= \mathrm{vec}\left(\int_{T_p} \boldsymbol{x}_n(\tau, t)\boldsymbol{S}^{\mathrm{H}}(t)\,\mathrm{d}t\right) \\ &= \sum_{r=1}^{K_T} \alpha_r(\tau)[\boldsymbol{a}(\phi_r) \otimes \boldsymbol{b}(\phi_r)] \\ &\quad + \sum_{i=1}^{K_I} \alpha_i(\tau)[\boldsymbol{a}(\phi_i) \otimes \boldsymbol{b}(\phi_i)] \\ &\quad + \sum_{j=1}^{J} \beta_j(\tau)\left[\mathbf{1}_M \otimes \boldsymbol{b}(\phi_j)\right] + \boldsymbol{e} \end{aligned} \tag{15}$$

where $\boldsymbol{e} = \mathrm{vec}\left(\int_{T_p} \boldsymbol{n}(t)\boldsymbol{S}^{\mathrm{H}}(t)\,\mathrm{d}t\right)$ is the $MN \times 1$ noise term, whose covariance matrix is $\boldsymbol{C}_e = \sigma_{n0}^2\boldsymbol{I}_{MN}$. Let $\boldsymbol{v}(\phi_r) = \boldsymbol{a}(\phi_r) \otimes \boldsymbol{b}(\phi_r)$, $\boldsymbol{v}(\phi_i) = \boldsymbol{a}(\phi_i) \otimes \boldsymbol{b}(\phi_i)$ and $\tilde{\boldsymbol{v}}(\phi_j) = \mathbf{1}_M \otimes \boldsymbol{b}(\phi_j)$ denote the $MN \times 1$ virtual steering vectors of the rth target, the ith interfering source and the jth jammer, respectively. For the discrimination of $\tilde{\boldsymbol{v}}(\phi_j)$ from $\boldsymbol{v}(\phi_r)$, the special case of $\phi_r = \phi_j = 0$ is not considered in our signal model. Then, (15) is rewritten as

$$z(\tau) = \sum_{r=1}^{K_T} \alpha_r(\tau)\boldsymbol{v}(\phi_r) + \sum_{i=1}^{K_I} \alpha_i(\tau)\boldsymbol{v}(\phi_i) + \sum_{j=1}^{J} \beta_j(\tau)\tilde{\boldsymbol{v}}(\phi_j) + \boldsymbol{e} \quad (16)$$

To annihilate the interference and jamming signal components simultaneously, the ideal $MN \times D(D \le MN)$ SFMM $\boldsymbol{B}$ is expected to meet the following requirements and meanwhile ensure the target distortionless response constraint for DOA estimation:

$$\begin{cases} \boldsymbol{B}^{\mathrm{H}}\boldsymbol{v}(\phi_i) = \boldsymbol{0} & i = 1, 2, \ldots, K_I \\ \boldsymbol{B}^{\mathrm{H}}\tilde{\boldsymbol{v}}(\phi_j) = \boldsymbol{0} & j = 1, 2, \ldots, J \end{cases} \quad (17)$$

In this ideal condition, the measured projection is obtained as follows:

$$\begin{aligned} \boldsymbol{y}'(\tau) = \boldsymbol{B}^{\mathrm{H}}\boldsymbol{z}(\tau) &= \boldsymbol{B}^{\mathrm{H}}\sum_{r=1}^{K_T} \alpha_r(\tau)\boldsymbol{v}(\phi_r) + \boldsymbol{B}^{\mathrm{H}}\boldsymbol{e} \\ &= \boldsymbol{B}^{\mathrm{H}}\sum_{r=1}^{K_T} \alpha_r(\tau)\boldsymbol{v}(\phi_r) + \boldsymbol{e}' \end{aligned} \quad (18)$$

where $\boldsymbol{e}' = \boldsymbol{B}^{\mathrm{H}}\boldsymbol{e}$ is the $D \times 1$ noise term with the $MN \times MN$ covariance matrix $\boldsymbol{C}_{e'} = \sigma_{n_0}^2\boldsymbol{B}\boldsymbol{B}^{\mathrm{H}}$. In light of the very dense grids in $\boldsymbol{\Omega}$ (*i.e.* Q is large enough), similar to (6), (18) can be extended to the discretised grids of $\boldsymbol{\Omega}$ and rewritten as

$$\boldsymbol{y}'(\tau) = \boldsymbol{B}^{\mathrm{H}}\sum_{q=1}^{Q} \gamma'_q(\tau)\boldsymbol{v}(\theta_q) + \boldsymbol{e}' = \boldsymbol{B}^{\mathrm{H}}\boldsymbol{\Xi}\boldsymbol{\gamma}'(\tau) + \boldsymbol{e}' \quad (19)$$

where $\boldsymbol{\Xi} = [\boldsymbol{v}(\theta_1), \boldsymbol{v}(\theta_2), \ldots, \boldsymbol{v}(\theta_Q)]$ (with size $MN \times Q$) is the constructed sparse basis and the $Q \times 1$ vector of SR-based coefficients is given by

$$\boldsymbol{\gamma}'(\tau) = [\gamma'_1(\tau), \gamma'_2(\tau), \ldots, \gamma'_Q(\tau)]^{\mathrm{T}} \quad (20)$$

where

$$\gamma'_q(\tau) = \begin{cases} \alpha_r(\tau) & \text{if } \theta_q = \phi_r \\ 0 & \text{otherwise} \end{cases} \quad (21)$$

and $\boldsymbol{\Gamma}' = \boldsymbol{B}^{\mathrm{H}}\boldsymbol{\Xi}$ with the size of $D \times Q$ stands for the corresponding sensing matrix. Then, (19) is expressed as

$$\boldsymbol{y}'(\tau) = \boldsymbol{\Gamma}'\boldsymbol{\gamma}'(\tau) + \boldsymbol{e}' \quad (22)$$

After L_s slow-time (pulses) measurements, we can have the multiple measurement vector (MMV) model as follows:

$$\begin{aligned} \boldsymbol{Y}' &= [\boldsymbol{y}'(1), \boldsymbol{y}'(2), \ldots, \boldsymbol{y}'(L_s)] \\ &= \boldsymbol{\Gamma}[\boldsymbol{\gamma}'(1), \boldsymbol{\gamma}'(2), \ldots, \boldsymbol{\gamma}'(L_s)] + [\boldsymbol{e}', \boldsymbol{e}', \ldots, \boldsymbol{e}'] \end{aligned} \quad (23)$$

It is worth noting that in view of the slow-time-varying characteristics of the radar signal, the SR-based coefficient vectors $\boldsymbol{\gamma}'(1), \boldsymbol{\gamma}'(2), \ldots, \boldsymbol{\gamma}'(L_s)$ of L_s measurements have the same sparsity, *i.e.* the values of the largest non-zero sparse coefficients are different, but the grid indexes in $\boldsymbol{\Omega}$ are the same. Furthermore, it means that the estimated DOA values corresponding to these grid indexes are the same.

For the above MMV model, we can take advantages of the relationship among the coefficient vectors to improve the reconstruction performance of signal. Sparse Bayesian learning (SBL) [17] and focal underdetermined system solver (FOCUSS) [18] are usually adopted to solve the recovery problem of MMV model. Owing to the larger computation complexity of SBL, FOCUSS is employed for the sparse recovery of MMV model in (23). Suppose that the recovered coefficient vectors are denoted as $\hat{\boldsymbol{\gamma}}'(1), \hat{\boldsymbol{\gamma}}'(2), \ldots, \hat{\boldsymbol{\gamma}}'(L_s)$, then the DOAs of targets can be finally estimated as follows:

$$\boldsymbol{g} = \frac{1}{L_s}\sum_{\tau=1}^{L_s} \| \hat{\boldsymbol{\gamma}}'(\tau) \|^2 \quad (24)$$

The angles in $\boldsymbol{\Omega}$ with the K_T largest non-zero sparse coefficients in $\boldsymbol{g}$ provide the DOA estimates of targets [19].

3 Adaptive SFMM design

Unfortunately, the ideal SFMM in (17) cannot be found directly. In this section, employing the first two beamspace matrix optimisation schemes for colocated MIMO radar in [13], three SFMM design approaches are proposed to suppress the unknown jamming in the SOI and the out-of-sector interference/clutter simultaneously, and meanwhile ensure the target's DOA estimation performance for colocated CS-MIMO radar. The SFMM design is inspired by the SSBM method that we summarise as follows.

In [4], discrete prolate spheroidal sequences were employed for transmitted beamspace dimension reduction and an SSBM is proposed for colocated MIMO radar. The idea is to maximise the ratio of the energy radiated within the SOI to the total radiated energy. Following this principle, the SSBM can be adopted for the target distortionless response in SOI and the suppression of out-of-sector interference/clutter. Similarly to [4, 13], let $\boldsymbol{W} = [\boldsymbol{w}_1, \boldsymbol{w}_2, \ldots, \boldsymbol{w}_D]$ be the $MN \times D$ beamspace matrix (see (25)) $\boldsymbol{w}_d$ ($d = 1, 2, \ldots, D$) denotes the $MN \times 1$ unit-norm weight vector. Then, we have the optimisation problem as (25), where h_d is the ratio of the energy radiated within the target SOI $\boldsymbol{\Theta}$ to the total energy radiated within the whole spatial domain $[-\pi/2, \pi/2]$, $\boldsymbol{A} = \int_{\boldsymbol{\Theta}}\boldsymbol{v}(\theta)\boldsymbol{v}^{\mathrm{H}}(\theta)\mathrm{d}\theta$ is a non-negative matrix. The last equality in (25) is due to the fact that $\boldsymbol{v}(\theta)$ obeys the Vandermonde structure

$$\int_{-\pi/2}^{\pi/2} \left|\boldsymbol{w}_d^{\mathrm{H}}\boldsymbol{v}(\theta)\right|^2 \mathrm{d}\theta = 2\pi\boldsymbol{w}_d^{\mathrm{H}}\boldsymbol{w}_d \quad (26)$$

As explained in [4], the orthogonality constraint $\boldsymbol{W}^{\mathrm{H}}\boldsymbol{W} = \boldsymbol{I}$ should be imposed for the maximisation of $\{h_d\}_{d=1}^{D}$ to avoid the trivial solution $\boldsymbol{w}_1 = \boldsymbol{w}_2 = \cdots = \boldsymbol{w}_D$. Then, optimisation p_1 is tantamount to find the eigenvectors of $\boldsymbol{A}$ that are associated with the D largest eigenvalues of $\boldsymbol{A}$. Suppose that $\{\boldsymbol{u}_d\}_{d=1}^{D}$ are the D principal eigenvectors of $\boldsymbol{A}$, then the SSBM $\boldsymbol{W}$ can be given by

$$p_1 = \begin{cases} \max\limits_{\boldsymbol{W}} h_d \quad d = 1, 2, \ldots, D \\ \text{s.t.} \qquad \boldsymbol{W}^{\mathrm{H}}\boldsymbol{W} = \boldsymbol{I} \\ \text{where} \quad h_d = \dfrac{\int_{\boldsymbol{\Theta}}\left|\boldsymbol{w}_d^{\mathrm{H}}\boldsymbol{v}(\theta)\right|^2 \mathrm{d}\theta}{\int_{-\pi/2}^{\pi/2}\left|\boldsymbol{w}_d^{\mathrm{H}}\boldsymbol{v}(\theta)\right|^2 \mathrm{d}\theta} = \dfrac{\boldsymbol{w}_d^{\mathrm{H}}\left(\int_{\boldsymbol{\Theta}}\boldsymbol{v}(\theta)\boldsymbol{v}^{\mathrm{H}}(\theta)\mathrm{d}\theta\right)\boldsymbol{w}_d}{\int_{-\pi/2}^{\pi/2}\left|\boldsymbol{w}_d^{\mathrm{H}}\boldsymbol{v}(\theta)\right|^2 \mathrm{d}\theta} \\ \qquad = \dfrac{\boldsymbol{w}_d^{\mathrm{H}}\boldsymbol{A}\boldsymbol{w}_d}{\int_{-\pi/2}^{\pi/2}\left|\boldsymbol{w}_d^{\mathrm{H}}\boldsymbol{v}(\theta)\right|^2 \mathrm{d}\theta} = \dfrac{\boldsymbol{w}_d^{\mathrm{H}}\boldsymbol{A}\boldsymbol{w}_d}{2\pi\boldsymbol{w}_d^{\mathrm{H}}\boldsymbol{w}_d} \end{cases} \quad (25)$$

$$\boldsymbol{W} = [\boldsymbol{u}_1, \boldsymbol{u}_2, \ldots, \boldsymbol{u}_D] \tag{27}$$

With regard to the selection of D, it depends on the width of $\boldsymbol{\Theta}$ and is regarded as the number of effective eigenvalues of $\boldsymbol{A}$, *i.e.* the sum of the D largest eigenvalues exceeding a certain percentage (*e.g.* 99%) of the total sum of all eigenvalues. Clearly, D is no smaller than the desired target number. By employing the SSBM in colocated MIMO radar, the out-of-sector interference/clutter can be attenuated. However, the attenuation levels of out-of-sector areas are limited. When the INR/CNR is large such as the scenario of Fig. 1, the SSBM fails to suppress effectively the interference/clutter. The case of SOI jamming is not considered. Herein, three SFMM design approaches are proposed for colocated CS-MIMO radar following the SSBM principles.

Owing to the uncertainty about the SOI jamming location in the presence of out-of-sector interfering sources and also following the energy focusing principle, we first design the adaptive SFMM as follows, in order to maximise the worst-case SOI jamming suppression, while the matrix difference between the desired SFMM $\boldsymbol{B}$ and the SSBM $\boldsymbol{W}$ is upper-bounded to be acceptable (similarity constraints between $\boldsymbol{B}$ and $\boldsymbol{W}$)

(see (28))

where $G_{\rm S}$ is the grid number of $\boldsymbol{\Theta}$ and $\xi > 0$ is the desired bound. With the constraint $\| \boldsymbol{B} - \boldsymbol{W} \|_{\rm F} \le \xi$, the transmitted power would mainly focus on the target SOI by employing $\boldsymbol{B}$ and the sidelobe attenuation levels of out-of-sector areas are almost the same as the ones introduced by employing $\boldsymbol{W}$, which would be limited.

For the powerful interference/clutter suppression, an alternative SFMM design approach is to constraint the attenuation levels of out-of-sector areas further [13]

(see (29))

where $G_{\rm O}$ is the grid number of out-of-sector areas $\bar{\boldsymbol{\Theta}}$, $\chi > 0$ refers to the desired level upper-bound of SOI jamming suppression, $\delta > 0$ is the parameter that characterises the worst acceptable attenuation of interference/clutter out-of-sector.

Note that an alternative adaptive approach for the problem p_3 is to maximise the level of SOI jamming suppression as much as possible, while the matrix difference and the attenuation levels of $\bar{\boldsymbol{\Theta}}$ are all acceptable based on the prior knowledge of power level of interference/clutter [13]

(see (30))

where ζ characterises the upper-bound of matrix difference, the minimum of which can be calculated from the problem p_3. It is worth pointing out that problems p_3 and p_4 are treated as SOC programming problems, which can be solved by the interior point algorithm [20]. To make the above optimisation problems more feasible and solvable by using CVX toolbox [21], we relax p_4, by introducing an auxiliary variable η, and by reformulating p_4 as a convex problem p_5. Finally, the problems p_2, p_3 and p_5 can all be solved by the 'infeasible path-following algorithm' in the CVX toolbox

(see (31))

In practise, $\boldsymbol{B}$ can be designed adaptively without the accurate angle information of targets, interfering sources and jammers, using only just rough information on the angle sectors, which can be obtained by the prior knowledge or some rough estimation methods. This allows us to simultaneously achieve target's DOA estimation and the joint suppression of SOI jamming and out-of-sector interference/clutter. Meanwhile, it should be emphasised that the last constraints of problems $p_3 - p_5$ are necessary only when there is some powerful interfering source/clutter located in the out-of-sector areas. When only the SOI jamming suppression is concerned or the interference/clutter is not powerful, these constraints can be removed or problem p_2 is adopted to design the adaptive SFMM.

4 Simulation results

In this section, the simulation results of three examples are presented and analysed to verify the effectiveness of jamming/interference joint suppression and target's DOA estimation. The simulation parameters are listed in Table 1. Two scenarios of SOI jamming with different and same DOAs as targets are considered in the presence of out-of-sector interfering sources. We take the virtual vector of the jth jammer as an example, the 16×1 transmit steering vector and the 8×1 receive steering vector are $[1, 1, \ldots, 1]^{\rm T}$ and $\boldsymbol{b}(\phi_j) = \left[1, {\rm e}^{j\pi \sin\phi_j}, \ldots, {\rm e}^{j7\pi \sin\phi_j}\right]^{\rm T}$, respectively. Then, the 128×1 virtual vector is $\tilde{\boldsymbol{v}}(\phi_j) = \left[\boldsymbol{b}^{\rm T}(\phi_j), \boldsymbol{b}^{\rm T}(\phi_j), \ldots, \boldsymbol{b}^{\rm T}(\phi_j)\right]^{\rm T}$. In (27), seven principal eigenvectors of $\boldsymbol{A}$ are selected to construct $\boldsymbol{W}$, *i.e.* $D = 7$. Moreover, the parameter in problem p_2 is set as $\xi = 0.55$ to constraint the similarities between $\boldsymbol{B}$ and $\boldsymbol{W}$ and optimise the sidelobe attenuation levels of out-of-sector areas as low as possible, and the ones in problems $p_3 - p_5$ are set as $\chi = 0.02$ and $\delta = 0.2$ for the enough deep notches/nulls for SOI jamming and the enough low sidelobe attenuation levels for out-of-sector interference, respectively. In practise, these parameters are selected based on the estimated

$$p_2 = \begin{cases} \min\limits_{\boldsymbol{B}} \ \max\limits_{j} & \| \boldsymbol{B}^{\rm H} \tilde{\boldsymbol{v}}(\theta_j) \|_2 \quad \theta_j \in \boldsymbol{\Theta} \quad j = 1, 2, \ldots, G_{\rm S} \\ {\rm s.t.} & \| \boldsymbol{B} - \boldsymbol{W} \|_{\rm F} \le \xi \end{cases} \tag{28}$$

$$p_3 = \begin{cases} \min\limits_{\boldsymbol{B}} & \| \boldsymbol{B} - \boldsymbol{W} \|_{\rm F} \\ {\rm s.t.} & \| \boldsymbol{B}^{\rm H} \tilde{\boldsymbol{v}}(\theta_j) \|_2 \le \chi \quad \theta_j \in \boldsymbol{\Theta} \quad j = 1, 2, \ldots, G_{\rm S} \\ & \| \boldsymbol{B}^{\rm H} \boldsymbol{v}(\bar{\theta}_i) \|_2 \le \delta \quad \bar{\theta}_i \in \bar{\boldsymbol{\Theta}} \quad i = 1, 2, \ldots, G_{\rm O} \end{cases} \tag{29}$$

$$p_4 = \begin{cases} \min\limits_{\boldsymbol{B}} \ \max\limits_{j} & \| \boldsymbol{B}^{\rm H} \tilde{\boldsymbol{v}}(\theta_j) \|_2 \quad \theta_j \in \boldsymbol{\Theta} \quad j = 1, 2, \ldots, G_{\rm S} \\ {\rm s.t.} & \| \boldsymbol{B} - \boldsymbol{W} \|_{\rm F} \le \zeta \\ & \| \boldsymbol{B}^{\rm H} \boldsymbol{v}(\bar{\theta}_i) \|_2 \le \delta \quad \bar{\theta}_i \in \bar{\boldsymbol{\Theta}} \quad i = 1, 2, \ldots, G_{\rm O} \end{cases} \tag{30}$$

$$p_5 = \begin{cases} \min\limits_{\boldsymbol{B}} & \eta \\ {\rm s.t.} & \| \boldsymbol{B}^{\rm H} \tilde{\boldsymbol{v}}(\theta_j) \|_2 \le \eta \quad \theta_j \in \boldsymbol{\Theta} \quad j = 1, 2, \ldots, G_{\rm S} \\ & \| \boldsymbol{B} - \boldsymbol{W} \|_{\rm F} \le \zeta \\ & \| \boldsymbol{B}^{\rm H} \boldsymbol{v}(\bar{\theta}_i) \|_2 \le \delta \quad \bar{\theta}_i \in \bar{\boldsymbol{\Theta}} \quad i = 1, 2, \ldots, G_{\rm O} \end{cases} \tag{31}$$

Table 1 Parameter description of colocated CS-MIMO radar, targets, interfering sources and jammers

radar	transmit element number	16	fast-time snapshot number L_f	512
	receive element number	8	slow-time snapshot number L_s	256
	angle grid interval	0.1°	SOI $\boldsymbol{\Theta}$	[10°, 25°]
	distance of two adjacent elements	$\lambda/2$	spatial areas out-of-sector $\bar{\boldsymbol{\Theta}}$	[−90°, 0°] ∪[35°, 90°]
target	DOAs	{12°, 23°}	SNR	10 dB
interfering sources	DOAs	{−40°, 55°}/ {[−90°: 20°: 0°]∪[35°: 20°: 90°]}	INR	25 dB
jammers	DOAs	[5°:10°: 25°]/ {12°, 18°, 23°}	JNR	50 dB

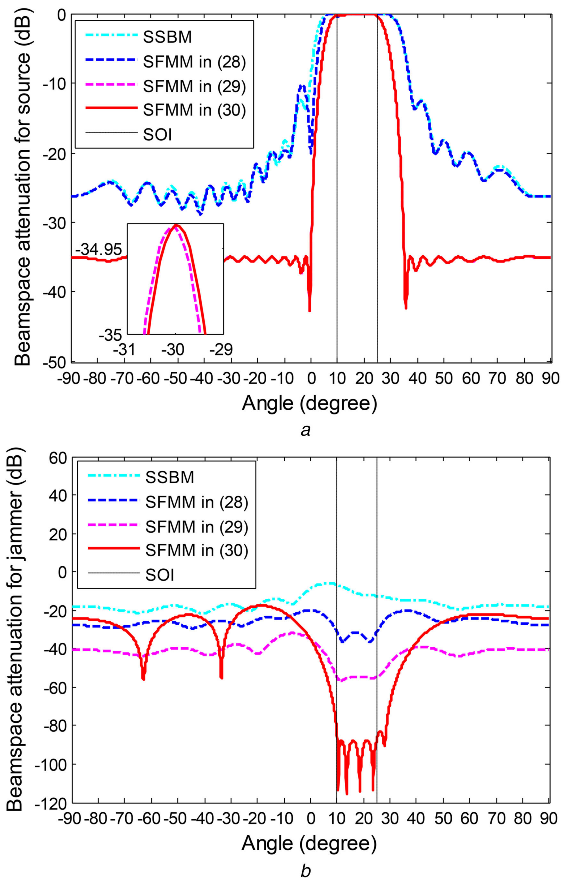

Fig. 3 *Beamspace attenuation of the designed SFMMs*
(a) For source, ***(b)*** For jammer

jamming-to-NR (JNR) and INR, while ensuring the target distortionless response in SOI. Smaller parameter values could obtain deeper notches or lower sidelobe attenuation levels, but also higher-level loss for a target in SOI. On the contrary, the SOI notches' levels for jamming would be higher in light of the estimated JNR or the out-of-sector attenuation levels for interference would be higher in light of the estimated INR, which lead to some interference or jamming residuals. With regard to the parameter ζ in problems p_4 and p_5, it can be obtained from the problem p_3.

4.1 DOA estimation and suppression effects

In the first example, the jammers are uniformly distributed and spaced 5° apart from each other in $\boldsymbol{\Theta}$. To show the SFMM effect intuitively, the beamspace attenuation is defined as [13]

$$f(\theta_q) = \frac{\| \boldsymbol{B}^{\mathrm{H}} \boldsymbol{m}(\theta_q) \|_2^2}{\| \boldsymbol{m}(\theta_q) \|_2^2} \quad q = 1, 2, \ldots, Q \tag{32}$$

where

$$\boldsymbol{m}(\theta_q) = \begin{cases} \boldsymbol{v}(\theta_q) & \text{for target} \\ \tilde{\boldsymbol{v}}(\theta_q) & \text{for jammer} \end{cases} \tag{33}$$

Fig. 3 shows the beamspace attenuation of SSBM [*i.e.* $\boldsymbol{B} = \boldsymbol{W}$ in (32)] and the proposed SFMMs in (28)–(30). We can find that some attenuation levels of SSBM for interfering sources are larger than −20 dB and the ones for SOI jammers are larger than −15 dB. Owing to the constraint optimisation for SOI jamming suppression, the ones of designed SFMM in (28) for jammers are smaller than −30 dB, but larger than −35 dB. When the power of SOI jamming and out-of-sector interference is not stronger, the designed SFMM in (28) would be effective; otherwise, the capability of jamming/interference joint suppression would be limited.

Benefiting from the constraints of out-of-sector areas and SOI jamming in (29) and (30), we can obtain lower-attenuation levels for the out-of-sector interference and SOI jamming simultaneously. Meanwhile, in light of the same constraints for $\bar{\boldsymbol{\Theta}}$ and the comparable constraints for $\boldsymbol{\Theta}$ [$\| \boldsymbol{B} - \boldsymbol{W} \|_F \le \zeta$, ζ is obtained from (29)], the beamspace attenuation levels for source using the SFMMs in (29) and (30) are almost the same. There is almost no attenuation for targets within the SOI in Fig. 3*a*, which ensures the accurate DOA estimation capability for targets.

Fig. 4 shows the estimated DOAs of targets employing the conventional CS-based method, SFMM-based method in [9] and the proposed SFMM in (30), respectively. Herein, to show the estimated DOA results clearly, the DOA coefficients of targets are set as 1.2.

In the second example, the jammers are assumed to be located at 12°, 18° and 23°, so two jammers are located at the same angles as the targets. The estimated targets' DOAs of the compared methods are shown in Fig. 5. It is seen that the proposed SFMM in (30) is also effective to suppress the powerful SOI jammers located in the same directions as targets. As shown in Figs. 4 and 5, disturbed by the powerful jamming and interference, the conventional CS method fails to estimate the DOAs of targets and the DOA estimation errors of the SFMM-based method in [9] are larger.

To test the DOA estimation performance of our proposed method in the presence of multiple interfering sources ($K_I > 2$), as shown in Fig. 6*a*, the interfering sources are assumed to be spaced 20° apart in the out-of-sector areas (*i.e.* [−90°: 20°: 0°]∪[35°: 20°: 90°]) and the estimated DOAs are shown in Fig. 6*b*. Contributed to the lower-attenuation levels for the out-of-sector areas, as shown in Fig. 3*a*, our proposed method can also estimate the DOAs of targets with smaller error, when the out-of-sector interference increases.

4.2 Performance versus signal-to-NR

To evaluate the performance of DOA estimation and jamming/interference joint suppression in the first example, the average root mean squared error (ARMSE) of the estimated DOAs, the probability of source resolution (PSR) and the signal-to interference-plus-jamming-plus-NR (SIJNR) are derived by Monte Carlo simulation. The number of trials is 200 for each signal-to-NR (SNR)

$$\mathrm{ARMSE} = \frac{1}{2} \sum_{r=1}^{2} \sqrt{\frac{1}{200} \sum_{i=1}^{200} \left(\hat{\phi}_r^i - \phi_r \right)^2} \tag{34}$$

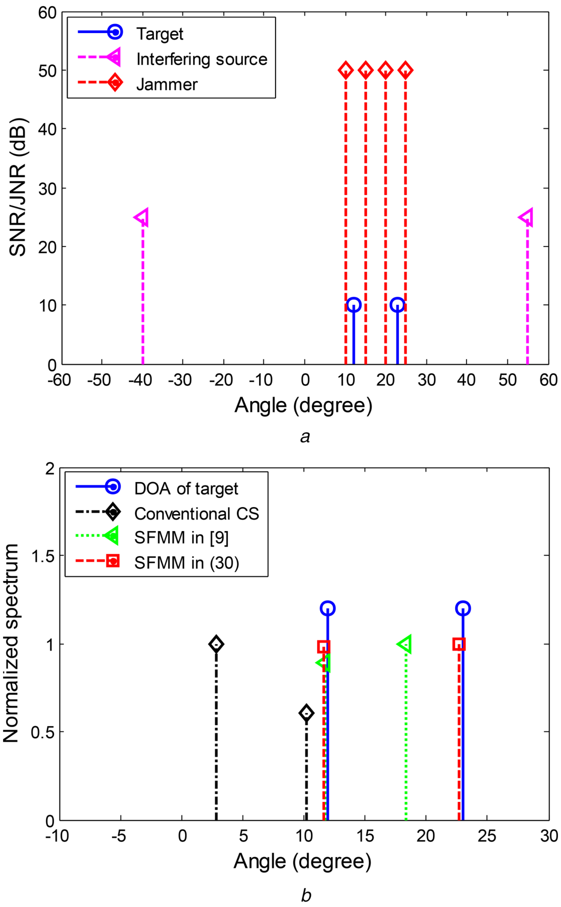

Fig. 4 *DOA estimation when the jammers space 5° apart in SOI*
(a) DOAs of targets, interfering sources and jammers, ***(b)*** Estimated DOAs of targets

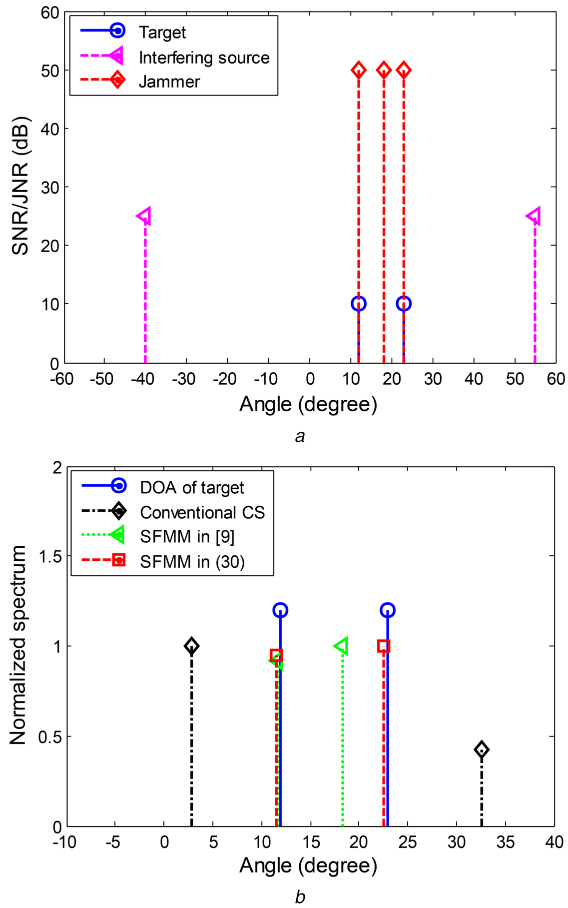

Fig. 5 *DOA estimation when jammers have the same DOAs as targets*
(a) DOAs of targets, interfering sources and jammers, ***(b)*** Estimated DOAs of targets

where $\hat{\phi}_r^i$ is the estimated value for the rth target in the ith run and ϕ_r denotes the exact DOA of the rth target. Moreover, we assume that the two targets can be resolved in the ith run if $\sum_{r=1}^{2} \left| \hat{\phi}_r^i - \phi_r \right| < \omega_{\text{beam}}$, where ω_{beam} is the width of the radar beam. Herein, we set the beamwidth as $\omega_{\text{beam}} = 2^{\circ}$ and the PSR ρ is defined as

$$\rho = \frac{1}{200} \sum_{i=1}^{200} p_i \tag{35}$$

where

$$p_i = \begin{cases} 1 & \text{if } \displaystyle\sum_{r=1}^{2} \left| \hat{\phi}_r^i - \phi_r \right| < 2^{\circ} \\ 0 & \text{otherwise} \end{cases} \tag{36}$$

p_i is defined as the PSR in the ith run. With regard to the output SIJNR, it can be written as equations below:

$$\begin{aligned} \text{SIJNR} &= \frac{E\left[\| \boldsymbol{B}^{\text{H}} \sum_{r=1}^{K_{\text{T}}} \alpha_r(\tau) \boldsymbol{v}(\phi_r) \|_2^2 \right]}{E\left[\| \boldsymbol{B}^{\text{H}} \left(\sum_{i=1}^{K_{\text{I}}} \alpha_i(\tau) \boldsymbol{v}(\phi_i) + \sum_{j=1}^{J} \beta_j(\tau) \tilde{\boldsymbol{v}}(\phi_j) + \boldsymbol{e} \right) \|_2^2 \right]} \\ &= \frac{E\left[\| \boldsymbol{B}^{\text{H}} \sum_{r=1}^{K_{\text{T}}} \alpha_r(\tau) \boldsymbol{v}(\phi_r) \|_2^2 \right]}{\| \boldsymbol{B}^{\text{H}} \boldsymbol{R}_{i+j+n} \boldsymbol{B} \|_2} \end{aligned} \tag{37}$$

$$\begin{aligned} \boldsymbol{R}_{i+j+n} = E\Bigg[& \left(\sum_{i=1}^{K_{\text{I}}} \alpha_i(\tau) \boldsymbol{v}(\phi_i) + \sum_{j=1}^{J} \beta_j(\tau) \tilde{\boldsymbol{v}}(\phi_j) + \boldsymbol{e} \right) \\ & \left(\sum_{i=1}^{K_{\text{I}}} \alpha_i(\tau) \boldsymbol{v}(\phi_i) + \sum_{j=1}^{J} \beta_j(\tau) \tilde{\boldsymbol{v}}(\phi_j) + \boldsymbol{e} \right)^{\text{H}} \Bigg] \end{aligned} \tag{38}$$

where $\boldsymbol{R}_{i+j+n}$ is the $MN \times MN$ interference-plus-jamming-plus-noise covariance matrix.

The ARMSE curves are shown in Fig. 7 by employing the conventional CS method, SFMM-based method in [9] and our proposed SFMM approaches in (28)–(30). Fig. 8 shows the corresponding PSR curves. The output SIJNRs of the proposed three SFMM approaches are shown in Fig. 9.

From Figs. 7–9, we can summarise the observations as follows:

(i) The performance of conventional CS method is worst and there is no obvious improvement with SNR. It ascribes to the inability of conventional CS method to cancel out the interference and jamming, which disturbs target's DOA estimation severely.

(ii) The SFMM-based method in [9] fails to jointly suppress the powerful interference and jamming. Unfortunately, no obvious improvement is obtained with larger SNR. Although the attenuation optimisation for spatial areas out-of-sector is considered, the attenuation levels are limited and the case of SOI jamming is omitted.

(iii) The design principle $\min_{\boldsymbol{B}} \max_r \| \boldsymbol{B}^{\text{H}} \boldsymbol{b}(\phi_r) - \boldsymbol{b}(\phi_r) \|_2$ in [9] only can guarantee that the amplitude difference between $\boldsymbol{B}^{\text{H}} \boldsymbol{b}(\phi_r)$ and $\boldsymbol{b}(\phi_r)$ is as smaller as possible; however, the phase and energy focus effects due to $\boldsymbol{B}$ are not taken into account. From (10)–(13), it can be seen that the DOA estimation of CS-MIMO radar mainly depends on the linear relationship between the measured signal $\boldsymbol{y}$ and the sensing matrix $\boldsymbol{\Gamma}$, and the phase distortionless response of $\boldsymbol{B}^{\text{H}} \boldsymbol{b}(\phi_r)$ could not be omitted in the design principle, so the joint

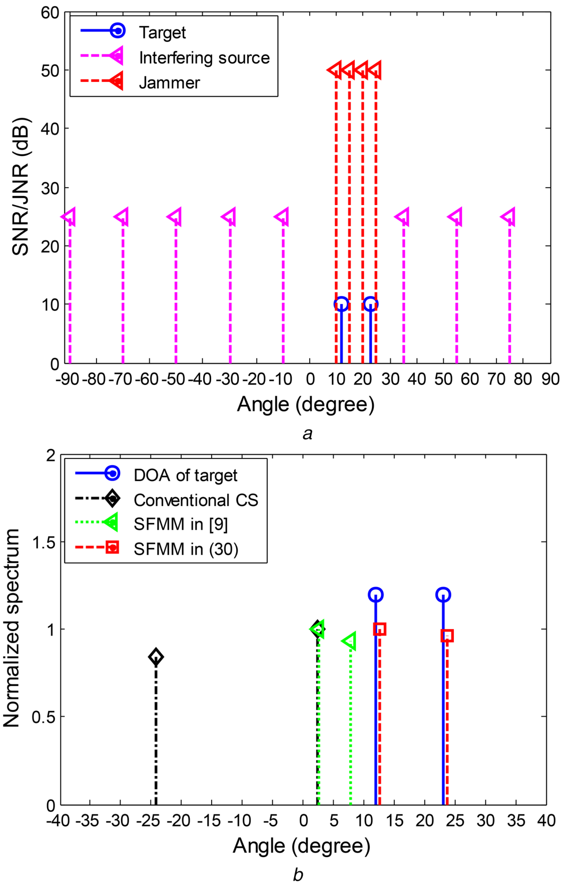

Fig. 6 *DOA estimation when the jammers space 5° apart in SOI and the interfering sources space 20° apart in out-of-sector areas*
(a) DOAs of targets, interfering sources and jammers, ***(b)*** Estimated DOAs of targets

suppression and DOA estimation performance of this method are limited.

(iv) Benefited from the joint optimisation of attenuation for SOI jamming and out-of-sector interference in (28)–(30), the DOA estimation and jamming/interference suppression of our proposed approaches outperform the others. It is worth noting that the constraint $\| \boldsymbol{B} - \boldsymbol{W} \|_{\mathrm{F}} \le \chi$ guarantees the similarity between $\boldsymbol{B}$ and $\boldsymbol{W}$. Following the energy focus principle of $\boldsymbol{W}$, the out-sector interference/clutter can be suppressed by employing the designed $\boldsymbol{B}$. Besides, the constraint $\| \boldsymbol{B}^{\mathrm{H}} \tilde{\boldsymbol{v}}(\theta_j) \|_2 \le \eta$ is expected to obtain the desired nulls or notches for SOI jamming suppression.

(v) The approach based on the SFMM in (30) has the best performance. When $\mathrm{SNR} \ge 5\,\mathrm{dB}$, $\mathrm{ARMSE} < 1^{\circ}$, $\rho = 1$ and $\mathrm{SIJNR} \ge 15\,\mathrm{dB}$. Especially, when $\mathrm{SNR} \ge 30\,\mathrm{dB}$, $\mathrm{ARMSE} < 10^{-2}$. This is due to: (a) the grid interval is 0.1° and the targets are all in-grid, (b) as we can see from Fig. 3 that notch attenuation gains of (30) for jammers are more than 85 dB, and the ones for sources out-of-sector areas are all more than 30 dB.

5 Conclusion

In this paper, three SFMM design approaches are derived which trade-off between SOI target distortion and jamming/interference suppression. In view of the unknown SOI jammers and non-cooperative interfering sources, each SFMM design problem is transformed to an SOC programming with the suppression constraints for the possible out-of-sector interference and SOI jamming. Meanwhile, it is expected to obtain the desired attenuation levels for out-of-sector interference and deep nulls or notches for SOI jamming. Simulation results demonstrate that the proposed SFMM design approaches not only can jointly suppress the SOI jamming and out-of-sector interference effectively, but also decrease the ARMSE, and improve the PSR and SIJNR. The proposed SFMM design approaches have good potential application for colocated CS-MIMO radar.

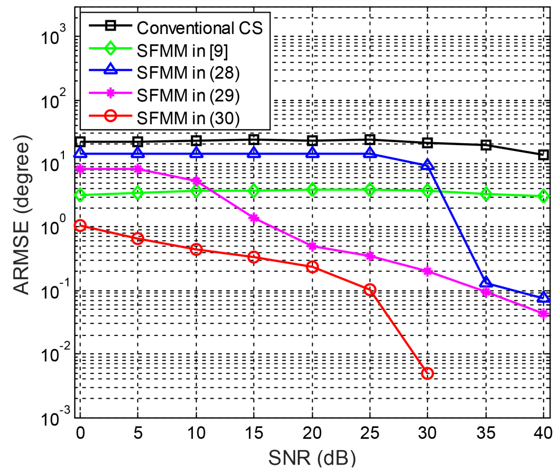

Fig. 7 *ARMSE of estimated DOAs versus SNR*

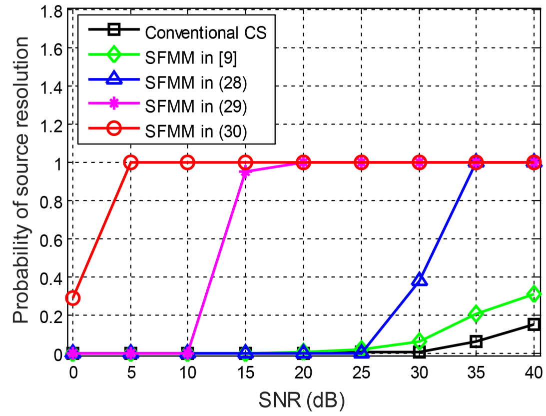

Fig. 8 *PSR curves versus SNR*

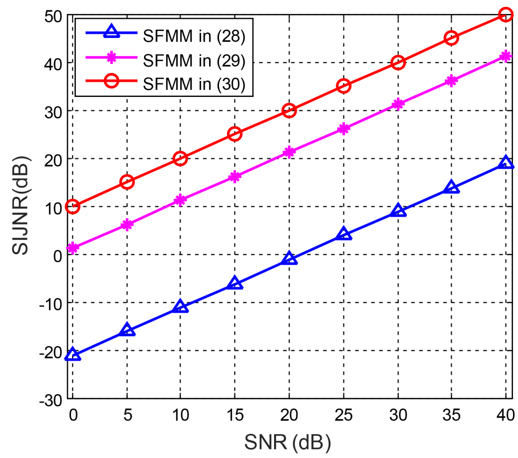

Fig. 9 *Output SIJNRs of our proposed approaches versus SNR*

6 Acknowledgments

The authors express their gratitude to the editor and anonymous reviewers for their helpful comments and suggestions that improved the quality of this paper. This work was supported by the National Natural Science Foundation of China (61471191, 61501233, 61671241, 61501228 and 61701046), the Aeronautical Science Foundation of China (20152052026), the Natural Science Foundation of Jiangsu (BK20140825), the Base Research foundation (NS2015040), the Funding of Jiangsu Innovation Program for Graduate Education (KYZZ16_0169), the Fundamental Research Funds for the Central University (3082017NP2017421) and also funded by China Scholarship Council (201606830017).

7 References

[1] Li, J., Stoica, P.: 'MIMO radar with colocated antennas', *IEEE Signal Process. Mag.*, 2007, **24**, (5), pp. 106–114

[2] Li, J., Stoica, P.: '*MIMO radar signal processing*' (Wiley-IEEE Press, New York, NY, 2009, 1st edn.)

[3] Wilcox, D., Sellathurai, M.: 'On MIMO radar subarrayed transmit beamforming', *IEEE Trans. Signal Process.*, 2012, **60**, (4), pp. 2076–2091

[4] Hassanien, A., Vorobyov, S.A.: 'Transmit energy focusing for DOA estimation in MIMO radar with colocated antennas', *IEEE Trans. Signal Process.*, 2011, **59**, (6), pp. 2669–2682

[5] Hassanien, A., Vorobyov, S.A.: 'Phased-MIMO radar: a tradeoff between phased-array and MIMO radars', *IEEE Trans. Signal Process.*, 2010, **58**, (6), pp. 3137–3151

[6] Yu, Y., Petropulu, A.P., Poor, H.V.: 'CSSF MIMO radar: compressive-sensing and step-frequency based MIMO radar', *IEEE Trans. Aerosp. Electron. Syst.*, 2012, **48**, (2), pp. 1490–1504

[7] Yu, Y., Petropulu, P.: 'CS-MIMO radars for through-the-wall imaging with simultaneous transmission'. IEEE Radar Conf. (RadarCon), OH, USA, May 2014, pp. 1439–1442

[8] Yu, Y., Sun, S.Q., Madan, R.N., *et al.*: 'Power allocation and waveform design for the compressive sensing based MIMO radar', *IEEE Trans. Aerosp. Electron. Syst.*, 2014, **50**, (2), pp. 898–909

[9] Tao, Y., Zhang, G., Zhang, Y.: 'Spatial filter measurement matrix design for interference/jamming suppression in colocated compressive sensing MIMO radars', *Electron. Lett.*, 2016, **52**, (11), pp. 956–958

[10] Yu, Y., Sun, S., Petropulu, A.P.: 'A capon beamforming method for clutter suppression in colocated compressive sensing based MIMO radars'. SPIE 8717, Compressive Sensing II, Baltimore, USA, April 2013, p. 87170

[11] Li, Y.Z., Vorobyov, S.A., Hassanien, A.: 'Robust beamforming for jammers suppression in MIMO radar'. IEEE Radar Conf. (RadarCon), OH, USA, May 2014, pp. 629–634

[12] Cox, H., Zeskind, R., Owen, M.: 'Robust adaptive beamforming', *IEEE Trans. Signal Process.*, 1987, **35**, (10), pp. 1365–1376

[13] Li, Y.Z., Vorobyov, S.A., Hassanien, A.: 'MIMO radar capability on powerful jammers suppression'. IEEE Int. Conf. Acoustics, Speech and Signal Processing (ICASSP), Florence, Italy, May 2014, pp. 5277–5281

[14] Zhang, J., Liu, N, Zhang, L.R., *et al.*: 'Active jamming suppression based on transmitting array designation for colocated multiple-input multiple-output radar', *IET Radar Sonar Navig.*, 2016, **10**, (3), pp. 500–505

[15] Li, Y.Z., Vorobyov, S.A., He, Z.S.: 'Terrain-scattered jammer suppression in MIMO radar using space-(fast) time adaptive processing'. IEEE Int. Conf. Acoustics, Speech and Signal Processing (ICASSP), Shanghai, China, May 2016, pp. 3026–3030

[16] Rossi, M., Haimovich, A.M., Eldar, Y.C.: 'Spatial compressive sensing for MIMO radar', *IEEE Trans. Signal Process.*, 2014, **62**, (2), pp. 419–430

[17] Ji, S.H., Xue, Y., Carin, L.: 'Bayesian compressive sensing', *IEEE Trans. Signal Process.*, 2008, **56**, (6), pp. 2346–2356

[18] Gorodnitsky, I.F., Rao, B.D.: 'Sparse signal reconstruction from limited data using FOCUSS: a re-weighted minimum norm algorithm', *IEEE Trans. Signal Process.*, 1997, **45**, (3), pp. 600–616

[19] Wang, Y., Leus, G., Pandharipande, A.: 'Direction estimation using compressive sampling array processing'. IEEE Workshop on Statistical Signal Processing, Cardiff, UK, September 2009, pp. 626–629

[20] Boyd, S., Vandenberghe, L.: '*Convex optimization*' (Cambridge University Press, New York, NY, 2004, 1st edn.)

[21] 'CVX: MATLAB software for disciplined convex programming, version 2.0 beta', Available at http://www.cvxr.com/cvx, accessed 4 December 2016